Cancer Immunology, Immunotherapy (2019) 68:1479–1492
https://doi.org/10.1007/s00262-019-02380-2

ORIGINAL ARTICLE

An optimized retinoic acid-inducible gene I agonist M8 induces immunogenic cell death markers in human cancer cells and dendritic cell activation

Luciano Castiello[1,5] · Alessandra Zevini[1] · Elisabetta Vulpis[2] · Michela Muscolini[1] · Matteo Ferrari[1] · Enrico Palermo[1] · Giovanna Peruzzi[3] · Christian Krapp[4] · Martin Jakobsen[4] · David Olagnier[4] · Alessandra Zingoni[2] · Angela Santoni[1,2] · John Hiscott[1]

Received: 7 December 2018 / Accepted: 15 August 2019 / Published online: 28 August 2019

Abstract

RIG-I is a cytosolic RNA sensor that recognizes short 5′ triphosphate RNA, commonly generated during virus infection. Upon activation, RIG-I initiates antiviral immunity, and in some circumstances, induces cell death. Because of this dual capacity, RIG-I has emerged as a promising target for cancer immunotherapy. Previously, a sequence-optimized RIG-I agonist (termed M8) was generated and shown to stimulate a robust immune response capable of blocking viral infection and to function as an adjuvant in vaccination strategies. Here, we investigated the potential of M8 as an anti-cancer agent by analyzing its ability to induce cell death and activate the immune response. In multiple cancer cell lines, M8 treatment strongly activated caspase 3-dependent apoptosis, that relied on an intrinsic NOXA and PUMA-driven pathway that was dependent on IFN-I signaling. Additionally, cell death induced by M8 was characterized by the expression of markers of immunogenic cell death-related damage-associated molecular patterns (ICD-DAMP)—calreticulin, HMGB1 and ATP—and high levels of ICD-related cytokines CXCL10, IFNβ, CCL2 and CXCL1. Moreover, M8 increased the levels of HLA-ABC expression on the tumor cell surface, as well as up-regulation of genes involved in antigen processing and presentation. M8 induction of the RIG-I pathway in cancer cells favored dendritic cell phagocytosis and induction of co-stimulatory molecules CD80 and CD86, together with increased expression of IL12 and CXCL10. Altogether, these results highlight the potential of M8 in cancer immunotherapy, with the capacity to induce ICD-DAMP on tumor cells and activate immunostimulatory signals that synergize with current therapies.

Keywords RIG-I · Interferons · Cancer immunotherapy · Immunogenic cell death · Dendritic cells

✉ Luciano Castiello
luciano.castiello@iss.it

✉ John Hiscott
john.hiscott@istitutopasteur.it

[1] Istituto Pasteur Italia-Cenci Bolognetti Foundation, Viale Regina Elena 291, 00161 Rome, Italy

[2] Department of Molecular Medicine, Sapienza University, Rome, Italy

[3] Center for Life Nano Science@Sapienza, Istituto Italiano di Tecnologia, Rome, Italy

[4] Department of Biomedicine, Aarhus University, Aarhus, Denmark

[5] Present Address: FaBioCell, Core Facilities, Istituto Superiore di Sanità, Rome, Italy

Abbreviations

7-AAD	7-Aminoactinomycin D
Ac-YVAD-CMK	Acetyl–tyrosyl-valyl-alanyl-aspartyl–chloromethylketone
APC	Allophycocyanin
APM	Antigen processing machinery
ATCC	American Type Culture Collection
BAX	Bcl-2-associated X protein
BD	Becton Dickinson
BH3	Bcl-2 homology 3
CARD	Caspase recruitment domain
CCCP	Carbonyl cyanide 3-chlorophenylhydrazone
CCL2	C-C motif chemokine ligand 2
CTFR	Cell trace far red
CXCL1	C-X-C motif ligand 1
CXCL10	C-X-C motif chemokine 10

DAMP	Damage-associated molecular patterns
EBV	Epstein–Barr virus
F-12K	Kaighn's modification of Ham's F-12 medium
FSC-A	Forward scatter-area
FSC-H	Forward scatter-height
GAPDH	Glyceraldehyde 3-phosphate dehydrogenase
Gy	Gray
HEPES	4-(2-Hydroxyethyl)-1-piperazineethanesulfonic acid
HLA-ABC	Human leucocyte antigens-A, B, and C loci
HMGB1	High-mobility group box 1
ICD	Immunogenic cell death
IDO1	Indoleamine-pyrrole 2,3-dioxygenase 1
IFNβ	Interferonβ
IFNAR1	Interferon α and β receptor subunit 1
IFN-I	Type-I interferon
IKK	IκB kinase
IRF3	Interferon regulatory factor 3
MAVS	Mitochondrial antiviral signaling protein
MDSC	Myeloid-derived suppressor cells
MiRNA	MicroRNA
MoDC	Monocyte-derived dendritic cells
P/S	Penicillin–streptomycin solution
PAMP	Pathogen-associated molecular patterns
PARP	Poly (ADP-ribose) polymerase
PRR	Pattern recognition receptors
PSMB8/9/10	Proteasome subunit beta type-8, -9, -10
PUMA	p53 upregulated modulator of apoptosis
RA	RIG-I agonist
RIG-I	Retinoic acid-inducible gene-I
RIP1	Receptor-interacting protein 1
RLU	Relative light units
SiRNA	Short interfering RNA
TAM	Tumor-associated macrophages
TAP1/2	Antigen peptide transporter 1, 2
TAPBP	Tapasin
TBK1	TANK-binding kinase 1
VSV	Vesicular stomatitis virus
Z-VAD-FMK	Carbobenzoxy-valyl-alanyl-aspartyl-[O-methyl]-fluoromethylketone

Introduction

Tumor cells use multiple strategies to escape immune surveillance and to generate an immunosuppressive and protumorigenic microenvironment [1]. During this "immunoediting escape phase", cancer cells become less visible to cells of the immune system by: (1) downregulation of HLA-ABC, co-stimulatory molecules and NK ligands; (2) secretion of immunosuppressive factors (such as PD-L1, Galectin 9, IDO1); and/or (3) chemoattraction of immunosuppressive cells such as regulatory T cells, myeloid-derived suppressor cells and tumor-associated macrophages (Treg, MDSC and TAM, respectively) [2]. Several strategies are currently being investigated to overcome the limitations of the immunosuppressive microenvironment and induce tumor cell death. Among these approaches, the use of compounds that mimic viral infection represents a promising strategy to pair cell death signals with immune activation events [3]. During viral infection in fact, cells sense pathogen-associated molecular patterns (PAMP) and damage-associated molecular patterns (DAMP) through a family of sensors, collectively named pattern recognition receptors (PRR), that activate multiple immune response pathways, and in some cases, lead to death of infected cells.

The retinoic acid-inducible gene-I (RIG-I) is a cytosolic PRR for short 5′ triphosphate double-strand RNA, with a crucial role in activating immune response against viral infection [4]. Upon recognition of viral RNA, RIG-I associates with the adaptor mitochondrial antiviral signaling protein (MAVS), via caspase recruitment domain (CARD)-mediated interactions that in turn activate TBK1 and the IKK complex [5]. TBK1 and IKK then lead to the activation of IRF3 and NF-κB, respectively, thus inducing the interferon (IFN) antiviral and inflammatory responses [6, 7]. RIG-I signaling can also trigger suicide of infected cells as an ultimate mechanism of protection that limits viral spread through at least three different mechanisms: IRF3-dependent induction of apoptotic genes [8]; IRF3-mediated induction of BAX-dependent mitochondrial apoptosis [9]; and direct RIG-I induction of necroptosis [10]. Such dual effects (i.e., induction of cell death and immune activation) render RIG-I agonists promising therapeutic compounds for cancer treatment. Indeed, preliminary results have already shown that RIG-I agonists can induce cell death in different tumor types and activate both innate and adaptive immunity against tumors in mouse models [11–15].

By modifying the length, structure and sequence of the 5′ end of Vesicular Stomatitis Virus (VSV) RNA, we developed and characterized a RIG-I agonist (named M8) that was 10–100-fold more potent in stimulating an

antiviral response, when compared to other agonists [16]. M8 potently blocked a variety of viral infections in vitro and in vivo, in part due to the activation of an innate immune response with greater breadth and intensity. Furthermore, M8 acted as a potent vaccine adjuvant against influenza, leading to high antibody titers and a Th1-skewing of immune responses [17]. In the present study, we tested the anti-cancer therapeutic potential of M8 by taking advantage of its dual ability to induce cell death and activate innate immunity. Our results demonstrate that stimulation of the RIG-I pathway by M8 induced an IFN-dependent intrinsic apoptosis in different cancer cells, characterized by multiple features of ICD, as well as an increased antigen processing capacity and strong activation of dendritic cells (DC).

Materials and methods

Cell lines and cultures

Mel1007, Mel120, and PC3 cells were grown in RPMI supplemented with 10% fetal bovine serum (FBS, Thermo Fisher Scientific) and 1% of penicillin–streptomycin solution (P/S, 10,000 U/ml penicillin and 10 mg/ml streptomycin sulfate, Euroclone). A549 cells were grown in Ham's F-12K (Kaighn's) Medium (Thermo Fisher Scientific) supplemented with 10% FBS and 1% of P/S. HCT116 cells were grown in McCoy's 5A (Modified) Medium (Thermo Fisher Scientific) supplemented with 10% FBS and 1% of P/S.

Generation of RIG-I agonists and transfection

M8, RIG-I agonists #1 and #2 (RA#1 and RA#2) were synthesized using Megascript T7 Transcription Kit (Thermo Fisher Scientific) with synthetic oligonucleotides (Eurofins Genomics) and following manufacturer instructions. Templates used were:

GAAATTAATACGACTCACTATAGACGAAGACCACAAAACCAGATAAAAAAAAAAAAAAAAAAAAAAAAATAATTTTTTTTTTTTTTTTTTTTTTTTTATCTGGTTTTGTGGTCTTCGTC and GACGAAGACCACAAAACCAGATAAAAAAAAAAAAAAAAAAAAAAAAAATTATTTTTTTTTTTTTTTTTTTTTTTTTATCTGGTTTTGTGGTCTTCGTCTATAGTGAGTCGTATTAATTTC for **M8**; TCAAACAGAGGCCGCATGCCTATAGTGAGTCGTATTA and GCATGCGGCCTCTGTTTGACTATAGTGAGTCGTATTA for **RA#1**; TACGTAAGCTGGATAGCGCTATAGTGAGTCGTATTA and GCGCTATCCAGCTTACGTATATAGTGAGTCGTATTA for **RA#2**.

For RA#1 and RA#2, the two templates were used to synthesize complementary RNAs that were annealed before transfection. Synthesized RNA was then purified using Nucleospin MiRNA Kit (Macherey-Nagel) and their concentration was assessed using Nanodrop 2000 (Thermo Fisher Scientific).

For transfection of all RA, Lipofectamine RNA/iMax (Thermo Fischer Scientific) was used following manufacturer instructions. The amount of Lipofectamine was optimized for each cell type to reduce toxicity: 1.5 µl/ml was used for Mel1007 cells, 2 µl/ml for HCT116, 3 µl/ml for PC3, Mel120 and A549. Both RNAiMAX and RA were diluted in Opti-Mem (Thermo Fisher Scientific). To remove the 5′ triphosphate group of M8, Calf Intestinal Alkaline Phosphatase (Thermo Fischer Scientific) was used following manufacturer instructions and RNA was then purified as above.

Reagents

The LDH cytotoxicity assay (Thermo Fischer Scientific) was used following manufacturer instructions. For cell death inhibition, Z-VAD-FMK (Santa Cruz Biotechnology) was used at a final concentration of 100 µM, Ac-YVAD-CMK (Sigma Aldrich) was used at a final concentration of 100 µg/ml (~ 180 µM), Necrostatin-1 (Cayman Chemical) was used at a final concentration of 50 µM; all the reagents were added to the culture immediately after transfection. For RIG-I silencing by siRNA, Mel1007 plated in 6-well plates were transfected with 80 pmol of RIG-I siRNA or control-siRNA-A (Santa Cruz Biotechnology) using Lipofectamine RNA/iMax. After 24 h, cells were transfected with M8 and viability assessed after 48 h. To block IFN-I signaling anti-interferon-α/β receptor (IFNAR1) Chain 2 Antibody (clone MMHAR-2, Merck Millipore) was added to the culture media immediately after M8-transfection to a final concentration of 1 µg/ml.

PBMC and DC differentiation

PBMC were isolated from anonymous healthy donor buffy coats by Ficoll Paque Plus (GE healthcare) following manufacturer instructions and cultured in RPMI supplemented with 10% certified FBS (Thermo Fisher Scientific) and 1% of P/S. For DC differentiation, monocytes were isolated from fresh PBMC by magnetic selection using CD14 MicroBeads (Miltenyi Biotec) and cultured in RPMI supplemented with 10% Certified FBS (Thermo Fisher Scientific), 1% of P/S, 50 ng/ml of GMCSF (Miltenyi) and 25 ng/ml of IL-4 (Miltenyi). After 5 days of culture, DC were used for the phagocytosis assay or stimulated for 24 h with supernatants of transfected Mel1007 cells.

NK CD107 degranulation and cytotoxicity assay

As the source of effector cells, PBMCs were isolated from three healthy donors by gradient centrifugation Lymphoprep (Nycomed, Oslo, Norway) and co-cultured for 10 days with the irradiated (30 Gy) EBV-transformed B cell line RPMI 8866 at 37 °C in a humidified 5% CO_2 atmosphere, as previously described [18]. On day 10, the cell population was routinely > 95% $CD56^+CD16^+CD3^-$, as assessed by immunofluorescence and flow cytometry. M8-transfected Mel1007 cells and K562 cells were then incubated with the effector cells at 37 °C for 2 h. Thereafter, cells were washed and incubated for 45′ at 4 °C with the lysosomal marker CD107a-APC, anti-CD3-APC-H7 and anti-CD56-PE to gate on NK cells. At the end of the incubation, cells were washed and analyzed by flow cytometry for the percentage of CD107a+ cells among the gated CD3−/CD56+ cells.

The effector NKL cells were labeled with CFSE and co-cultured for 4 h with target Mel1007 transfected or not with M8 for 48 h or K562 cells at several Effector–Target ratios for 4 h at 37 °C. Cells were then washed and cytotoxicity was assessed by flow cytometry to analyze viable cells using 7-AAD among the $CFSE^-$ cells.

Phagocytosis assay

Mel1007 cells were labeled with Cell Trace Far Red (CTFR) (Thermo Fischer Scientific) and transfected with M8 for 48 h. Cells were then co-cultured at a 1:1 ratio with DC for 4 h. Cells were then washed and labeled with anti-CD209-PE and 7-AAD, and analyzed by flow cytometry to assess $CTFR^+$ cells among live $CD209^+$ cells.

Flow cytometry

Viability was assessed by gating 7-AAD exclusion over FSC-A plots on FSC-A vs FSC-H gated singlet cells. To evaluate early versus late apoptosis, cells were labeled with Annexin-V-APC (Biolegend) and 7-AAD in a solution of HEPES 0.01 M (Sigma Aldrich), NaCl 140 mM (Sigma Aldrich), CaCl2 2.5 mM (Sigma Aldrich) following manufacturer instructions. Mitochondrial depolarization was assessed by JC-1 staining (Thermo Scientific); after M8 treatment, JC-1 was added to a final concentration of 2.5 µM; cells were incubated in the dark at 37 °C for 15 min before cytometric analysis. The gating strategy was based on cells treated with the mitochondrial depolarization reagent carbonyl cyanide 3-chlorophenylhydrazone (CCCP).

To stain for calreticulin, cells were washed twice with cold PBS, fixed for 5′ in 0.25% paraformaldehyde, washed twice in cold PBS and incubated for 20′ with anti-calreticulin Ab (PA3900, Thermo Fischer Scientific). Labeled cells were then washed twice and incubated with AlexaFluor488-labeled secondary Ab for 30′ on ice (Abcam—ab150077). At the end of the incubation, cells were washed twice and re-suspended in a PBS solution containing 7-AAD. As a positive control, cells treated with Mitoxantrone 1 µM (Sigma Aldrich) were used. Only live cells were analyzed; dead cells were removed based on 7-AAD staining.

Staining for other cell surface markers was performed using standard incubation protocols and staining with anti-HLA-ABC-PE, anti-HLA-DR-APC (21388996) (both from Immunotools), anti-CD86-Brilliant Violet 421 (305426) and anti-CD209-PE (330106) (both from Biolegend), anti-CD80-FITC (557226), anti-CD3-APC-H7 (clone SK7), anti-CD56-PE (clone NCAM16.2), anti-CD107a-APC (clone H4A3) (all from BD Biosciences) antibodies. All the experiments were performed on BD FacsCanto II (BD Biosciences).

Quantitative PCR

RNA was isolated by column separation using the RNeasy Kit (Qiagen) following manufacturer's instructions and the concentration was measured with Nanodrop 2000 (Thermo Fischer Scientific). 350 ng of RNA was used for cDNA synthesis using the High-Capacity cDNA Reverse Transcription Kit (Thermo Fischer Scientific). Quantitative PCR was then performed using Taqman Fast Advanced MasterMix with Taqman probes or Universal ProbeLibrary Probes (Roche) with specific primers designed using the Roche Lifescience Assay Design Center (https://lifescience.roche.com/en_it/brands/universal-probe-library.html#assay-design-center) on a StepOnePlus Real-Time PCR System (Thermo Fischer Scientific). A relative quantification method was used, with GAPDH as housekeeper gene.

Magnetic Luminex assay

Supernatants of M8-transfected Mel1007 cells were analyzed on a 96-well plate for the presence of the following analytes: CCL2, CXCL1, CXCL10, and IFNβ. The fluorescence responses and concentrations of cytokines were obtained using a human premixed Multi-Analyte kit (R&D systems), and analyzed with a MAGPIX system and the accompanying xPONENT Software. All reagents were provided with the kit and were prepared according to the manufacturer's recommendations; reconstituted standards were serially diluted 1:3 in calibrator diluent, which was used as background. A microparticle cocktail, biotin-antibody cocktail, and streptavidin-PE were diluted in their specific buffers immediately before the assay. The Luminex protocol was followed exactly; 50 µl of sample and standard were incubated for 2 h with 50 µl of microplate cocktail, then the plate was washed and 50 µl of biotin-antibody cocktail was

added. After 1-h incubation, the plate was washed and 50 µl of streptavidin-PE was added for 30′, followed by a final wash and resuspension in 100 µl of wash buffer. All incubations were performed at room temperature on a microplate shaker at 800 rpm. Both standards and samples were tested in duplicate. The concentration values and detection limits were determined from standard curves generated from each kit's standards using the weighted 5PL curve fitting procedure. To maximize the number of concentration values available for analysis, the extrapolated values were included.

HMGB1 ELISA

Supernatants of Mel1007, HCT116 and PC3 cells transfected or not with M8 for 48 h were analyzed for HMGB1 levels using HMGB1 ELISA kit (ST51001, IBL international) following manufacturer instructions and absorbance measured with the iMark™ Microplate Absorbance Reader (Bio-Rad). As a positive control, cells treated with Mitoxantrone 1 µM (Sigma Aldrich) were used.

ATP release

Extracellular ATP levels were measured by the luciferin-based ENLITEN ATP Assay (Promega, Madison, WI, USA), following the manufacturer's instructions, and light intensity was measured using the Glomax luminometer. Briefly, 100 µl of undiluted supernatant was dispensed in duplicate in an opaque-walled 96-well plate; an equal volume of rL/L reagent was added to each well by an injection system, and a 2-s delay time after injection and 10-s RLU signal integration time were used to record the light signals resulting from the luciferase reactions.

Statistical analysis

Graphs and statistical analyses were performed using GraphPad Prism 6. Depending on the type of data to be analyzed, a one-way ANOVA or two-way ANOVA was used correcting multiple comparisons with Tukey's test, or standard *t* test using Sidak correction for multiple comparisons.

Results

Sequence-optimized RIG-I agonist M8 potently induced cell death in melanoma cancer cells

To assess the potential of M8 as an anti-cancer agent, we initially analyzed its ability to induce cell death in the melanoma cell line Mel1007. Significant levels of cell death were observed with concentrations of M8 higher than 100 ng/ml (Fig. 1a, b). To determine the specificity of M8 to induce RIG-I-directed cell killing, the 5′ triphosphate group of M8 was removed by calf intestinal phosphatase, resulting in a dramatic reduction in cell death (50% vs 3.7%) (Fig. 1c). A similar result was observed when RIG-I expression was silenced with siRNA against RIG-I for 24 h prior to M8 treatment. Indeed, M8-directed cell death was reduced to control levels in RIG-I silenced cells (from 30 to 9.5%) (Fig. 1d), thus supporting the observation that the 5′ triphosphate moiety is required to maintain specificity for RIG-I [6, 16].

Next, the capacity of M8 to induce cell death was compared to other RIG-I agonists previously shown to induce cell death in cancer cells [11, 15]. Among the compounds tested, M8 proved to be the strongest inducer of cell death in Mel1007 (58% vs 11 and 8%) (Fig. 1e). Moreover, M8 was effective in inducing cell death in a variety of other cancer cell lines, including metastatic melanoma Mel120, lung adenocarcinoma A549, colon carcinoma HCT116, prostate carcinoma PC3 (Fig. 1f) (40%, 75%, 45%, and 33%, respectively), indicating that cell death pathways activated by M8 were intact in other cancer cell types. The toxicity of M8 was also evaluated in PBMC, and M8 led to minimal levels of cell death, even at the highest dose (Fig. 1g), thus indicating that M8 toxicity was selective for cancer cells rather than normal cells [12]. Altogether, these results indicate that M8 activation of RIG-I induced cell death in different cancer cell types, while displaying limited toxicity in non-cancerous cells.

M8 induction of the IFN-I-dependent intrinsic apoptotic pathway

Next, the kinetics of induction of apoptosis was evaluated by annexin V staining at different times after M8 treatment. As shown in Fig. 2a, Mel1007 treated with M8 began showing apoptotic features as early as 16 h post transfection, with high percentages of early apoptotic cells between 24 and 30 h; by 48 h, most of the cells were dead, indicating that the mechanisms leading to cell death are initiated within the first 24 h. Several pharmacological inhibitors of cell death pathways were used to explore the specific nature of M8-mediated cell death. The pan-caspase inhibitor Z-VAD significantly reduced M8-induced cell death (from 44 to 19%) in a caspase 3-dependent manner, whereas caspase 1-dependent pyroptosis or necroptosis through the RIP1 kinase was ruled out, based on the use of the caspase 1 inhibitor YVAD or the necroptosis inhibitor necrostatin 1 (Fig. 2b). Cleavage of caspases 3 and 9 was detected by immunoblot at 24 h post treatment, together with cleavage of the downstream target PARP (Fig. 2c), indicating that M8-induced cell death involved the intrinsic apoptotic pathway. Mitochondrial depolarization was analyzed by JC1 staining at 24 h post treatment; as shown in Fig. 2d, M8 treatment of Mel1007

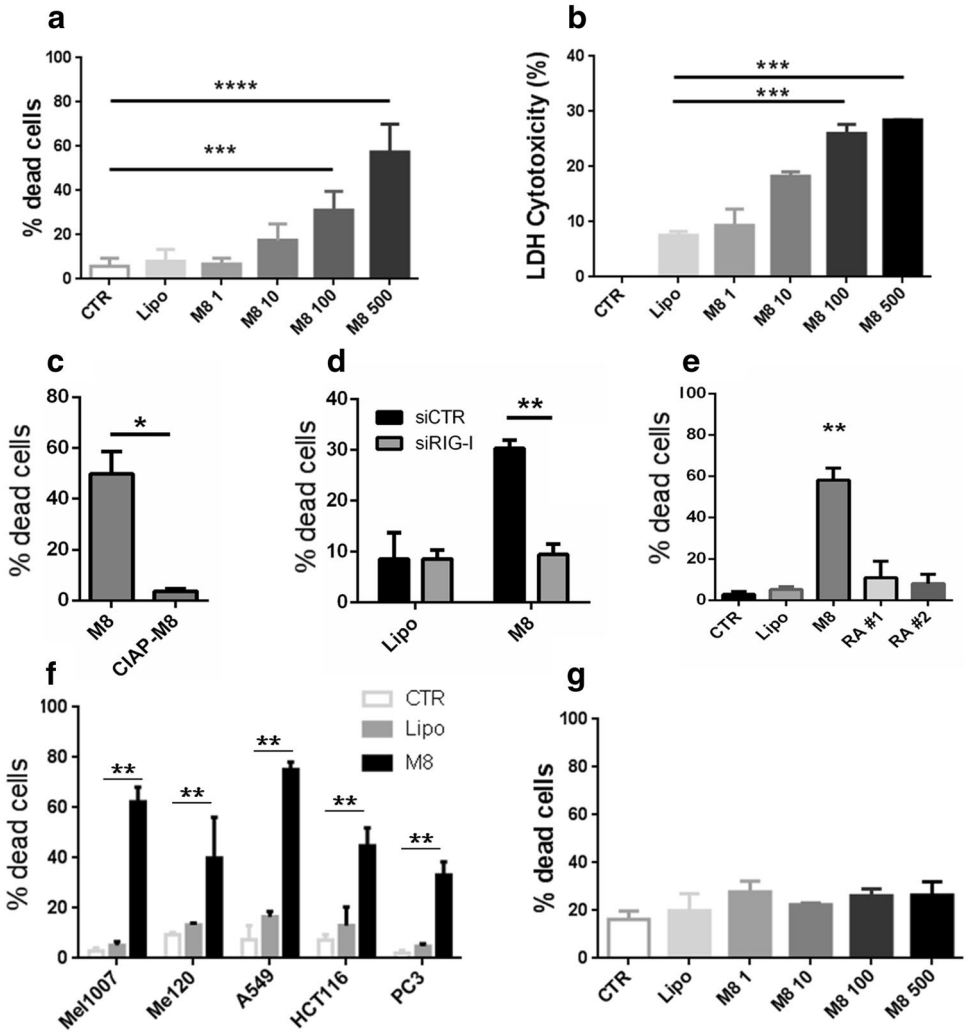

Fig. 1 RIG-I agonist M8 induces cell death in cancer cells. **a** Viability of Mel1007 cells transfected with different amounts of M8 (1–500 ng/ml) for 48 h was assessed by 7-AAD exclusion by flow cytometry; **b** LDH based cytotoxicity was measured in Mel1007 cell supernatants transfected with different amounts of M8 (1–500 ng/ml) for 48 h, the percentage cytotoxicity was calculated as the ratio of spontaneous-normalized LDH activity over normalized maximum control, as per manufacturer instructions; **c** viability of Mel1007 cells transfected with M8 or 5′ dephosphorylated M8 (CIAP-M8) (500 ng/ml) for 48 h, assessed by 7-AAD exclusion by flow cytometry; d) Viability of Mel1007 cells pretreated for 24 h with siRNA specific for RIG-I, and then transfected with M8 (500 ng/ml) for 48 h; **e** viability of Mel1007 cells transfected with the indicated RIG-I agonists (500 ng/ml), untreated, or transfected only with lipofectamine for 48 h; **f** viability of metastatic melanoma Mel120, lung adenocarcinoma A549, colon carcinoma HCT116, and prostate carcinoma PC3 transfected with 500 ng/ml of M8 for 48 h; **g** viability of PBMC transfected with different doses of M8 (1–500 ng/ml) for 48 h, assessed by 7-AAD exclusion by flow cytometry. $*P<0.05$; $**P<0.01$; $***P<0.001$

cells increased the percentage of cells exhibiting disrupted mitochondria. Next, to understand the pro-apoptotic factors involved in M8-induced cell death, we analyzed gene expression levels of the pro-apoptotic genes NOXA and PUMA. Notably, both genes were significantly induced upon M8 transfection (Fig. 2e, f); however, while PUMA expression levels were induced threefold, NOXA gene expression was induced approximately 100-fold.

To evaluate whether the apoptosis induced by M8 was modulated by type I IFN (IFN-I), cell death levels were evaluated in M8-treated Mel1007 cells in the presence of IFNAR1 blocking antibodies. As shown in Fig. 3a, cell death induced by M8 was inhibited by IFNAR1 blocking antibodies (21% vs 57%), thus demonstrating the requirement for IFN-I production and indicating that secreted IFN-I contributed to apoptosis. Consistent with this observation, the blockade of IFN-I signaling with IFNAR1 blocking antibodies inhibited pro-apoptotic gene expression and reduced the levels of PUMA and NOXA in M8-treated cells (1.4- vs 2.6-fold for PUMA, 45- vs 110-fold for NOXA) (Fig. 3b, c). Altogether, these results indicate that M8 induced an intrinsic apoptotic pathway in Mel1007 cells that relied on

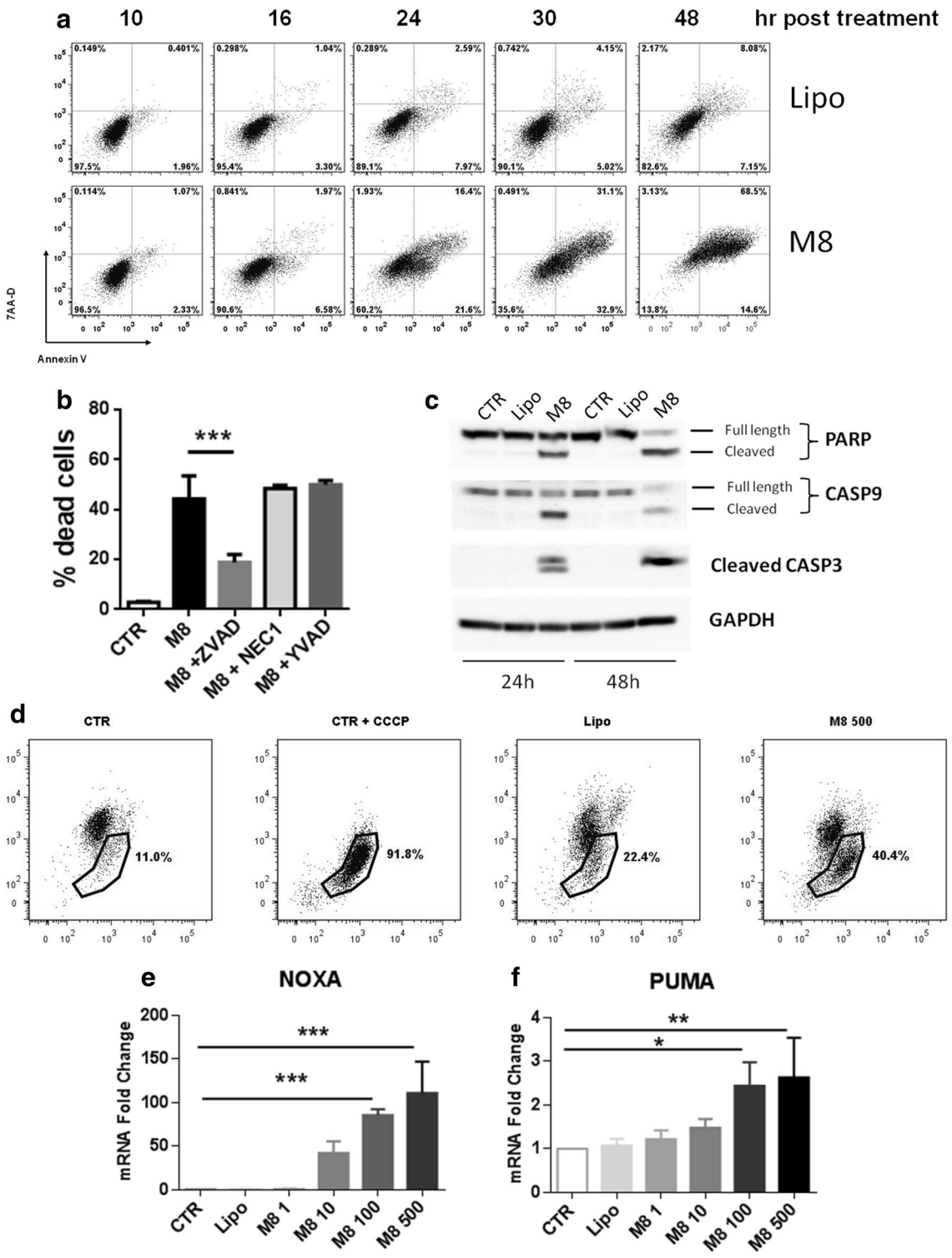

Fig. 2 M8 activates intrinsic apoptosis driven by PUMA and NOXA. **a** Flow cytometry evaluation of annexin V/7-AAD positivity of Mel1007 cells transfected with M8 (500 ng/ml) assessed at 10, 16, 24, 32 and 48 h; **b** viability of Mel1007 cells transfected for 48 h with M8 and treated with pan-caspase inhibitor ZVAD-FMK (100 μM), caspase 1 inhibitor YVAD-FMK (50 μg/ml), and the necroptosis inhibitor necrostatin 1 (100 μM); **c** western blot of Mel1007 cells transfected for 24 or 48 h with M8 (500 ng/ml); **d** Analysis of the percentage of Mel1007 cells showing monomeric JC-1, an indicator of mitochondria depolarization, at 24 h after transfection. CCCP was used as a positive control and added 30′ before the analysis; **e** expression levels of NOXA gene in Mel1007 cells 24 h after transfection with the indicated doses of M8; **f** expression levels of PUMA gene in Mel1007 cells 24 h after transfection with the indicated doses of M8. $^{*}P < 0.05$; $^{**}P < 0.01$; $^{***}P < 0.001$

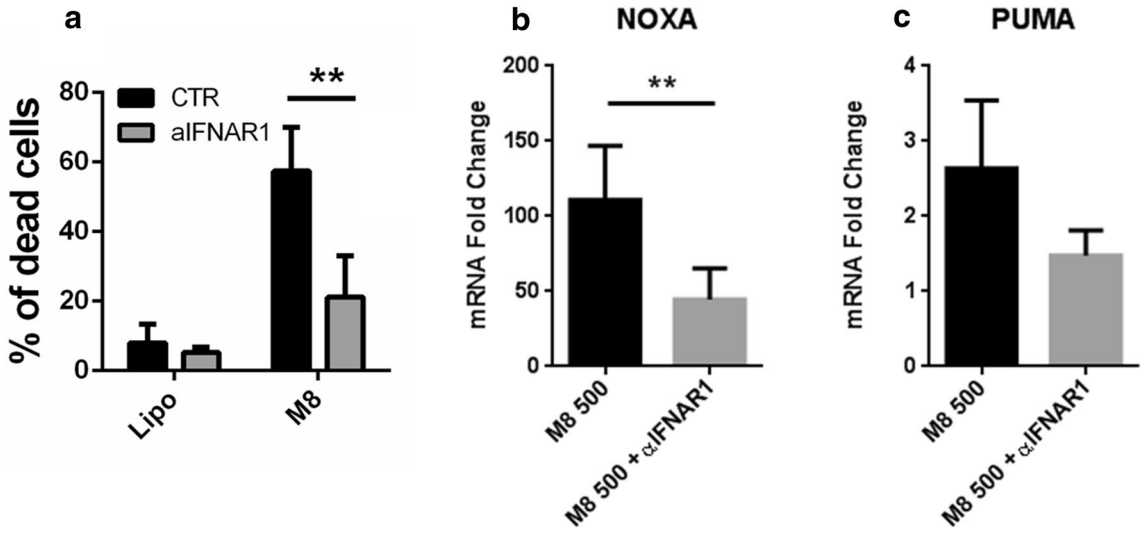

Fig. 3 M8-induced apoptosis relies on IFN-I signaling. **a** Viability of Mel1007 cells transfected with M8 (500 ng/ml) and treated with IFNAR1 blocking antibody (1 µg/ml) for 48 h; **b**, **c** expression levels of NOXA and PUMA genes, respectively, in Mel1007 cells 24 h after transfection with M8 500 ng/ml treated with IFNAR1 blocking antibody for 48 h (1 µg/ml). Fold changes were calculated over untreated Mel1007 cells. $^{**}P < 0.01$

IFN-I-dependent induction of PUMA and NOXA. The levels of residual apoptosis indicated that IFN-independent mechanisms may also contribute to M8-induced cell death [6, 12].

M8-induced markers of ICD-DAMP

Given its ability to mimic aspects of virus infection, M8 induced a RIG-I-dependent cytokine response; IFNβ transcript levels increased proportionally with increased concentration of M8 (10, 100, 500 ng/ml), and the downstream chemokine CXCL10 was induced dramatically (up to 10^3–10^4-fold). Addition of IFNAR1 blocking Ab reduced transcript levels, although residual cytokine mRNA was detected (Fig. 4a, b). Since IFNβ and CXCL10 are two critical factors required for ICD [19], we next determined the potential of M8 to induce the complete chemokine signature of ICD (i.e., CCL2, CXCL1, CXCL10 and IFNβ) by a multiplex ELISA assay. Notably, all cytokines tested displayed a dose-dependent and statistically significant increase, as measured in the supernatant of M8-treated Mel1007 versus control (Fig. 4c). Next, we assessed whether cell death induced by M8 displayed other features of ICD, such as exposure of calreticulin on the cell membrane, secretion of High Mobility Group Box 1 (HMGB1) and ATP release. As shown in Fig. 4d, M8 induced the surface exposure of calreticulin at levels comparable to the ICD inducer mitoxantrone in Mel1007 cells (Fig. 4d). Similar results were also observed in the HCT116 and PC3 cell lines (data not shown). Another marker of ICD, HMGB1 release was increased ~ 3-fold after M8 treatment in Mel1007 cells (Fig. 4e). HCT116 and PC3 cancer cells also induced ICD markers after M8 treatment (data not shown). Finally, ATP was measured in the extracellular supernatants of Mel1007 cells using a luciferase-based assay, revealing a > 500-fold increase in ATP release after M8 treatment (Fig. 4f). Altogether, these results demonstrate that M8 induced caspase 3-dependent cell death characterized by the induction of multiple ICD-DAMP.

M8 triggering of RIG-I represses NK activity and upregulates antigen processing machinery

Having observed the activation of several markers of ICD in cancer cells stimulated by M8, we next sought to determine if pathways downstream of RIG-I activation also generated signals crucial for immune cell recognition. The induction of NK cell activating signals on Mel1007 was evaluated using mid-range doses of M8 to ensure strong RIG-I activation and minimize cell death. As shown in Fig. 5a, most activating NK ligands were increased on the Mel1007 cell surface after M8 treatment, although not to a statistically relevant level. However, when NK degranulation and cytotoxic activities were measured, a clear inhibition of NK activity was observed. In fact, both CD107 exposure on the NK surface and the percentage of dead target cells after co-culture of NK and M8-Mel1007 cells indicated that M8 reduced NK activity when compared to negative or positive control cells (Fig. 5b, c), thus suggesting the potential involvement of inhibitory surface markers. In fact, a consistent induction of an NK inhibiting marker—HLA-ABC expression—was observed after M8 treatment (Fig. 5d) and was associated with a general increase in the activity of the antigen processing machinery (APM).

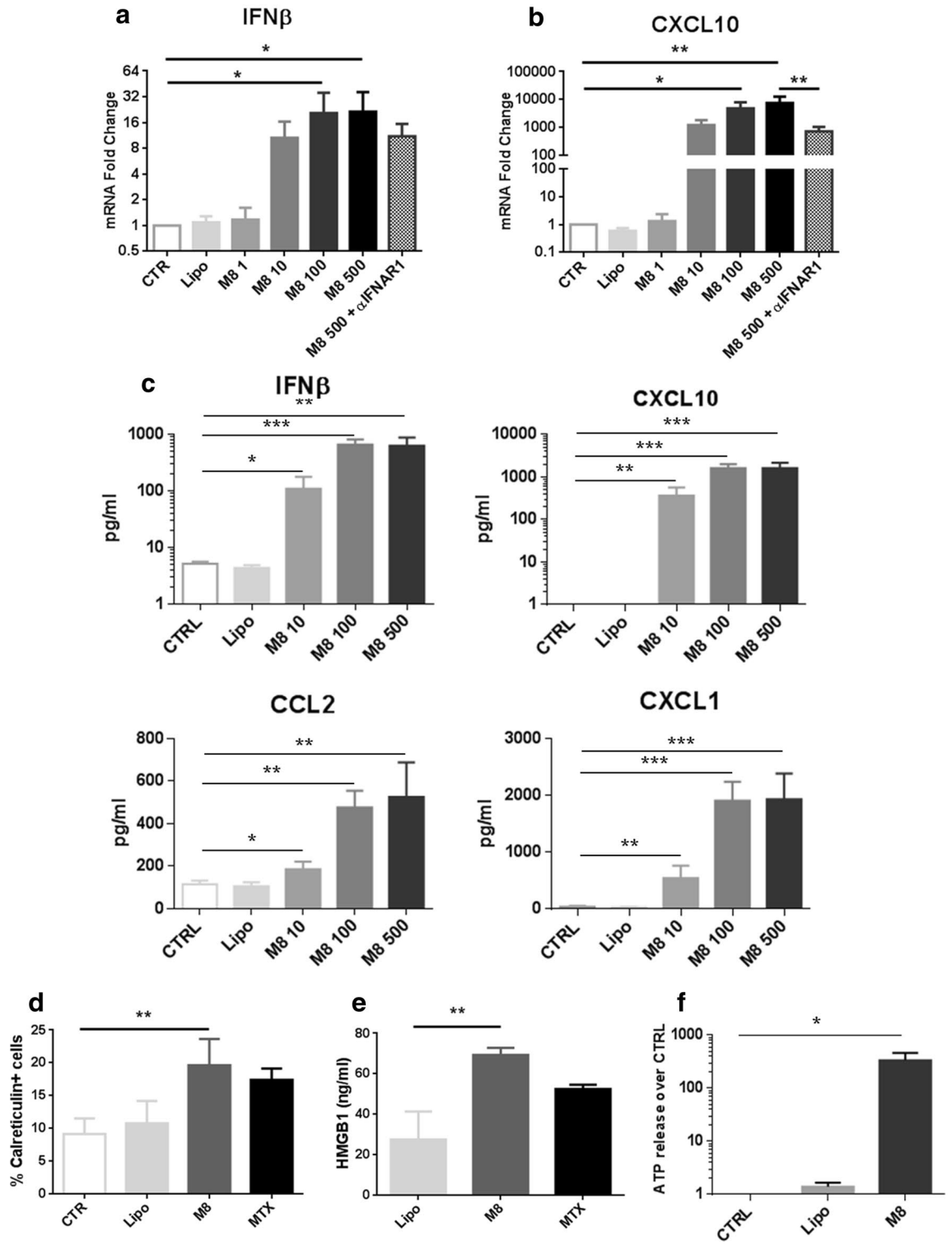

Fig. 4 M8 induces ICD-DAMP in cancer cells. **a**, **b** Expression of IFNβ and CXCL10 mRNA induced in Mel1007 cells at 24 h after transfection with different concentrations of M8 (10–500 ng/ml) or addition of IFNAR1 blocking antibody (1 μg/ml), expressed as fold increase over control cells; **c** analysis by Magnetic Luminex assay of the concentration (pg/ml) of chemokines CCL2, CXCL1, CXCL10, and IFNβ in supernatants of Mel1007 cells stimulated for 24 h with M8 (10, 100, and 500 ng/ml); **d** calreticulin expression as assessed by percentage of positive cells in Mel1007 30 h after transfection with M8 (500 ng/ml); mitoxantrone (1 μM) was used as positive control; **e** HMGB1 levels assessed by ELISA in supernatants of Mel1007 cells transfected with M8 (500 ng/ml) for 48 h; mitoxantrone (1 μM) was used as positive control; **f** ATP release by Mel1007 cells transfected with M8 (500 ng/ml) for 48 h as assessed in culture supernatants by luciferase-based test. $*P<0.05$; $**P<0.01$; $***P<0.001$

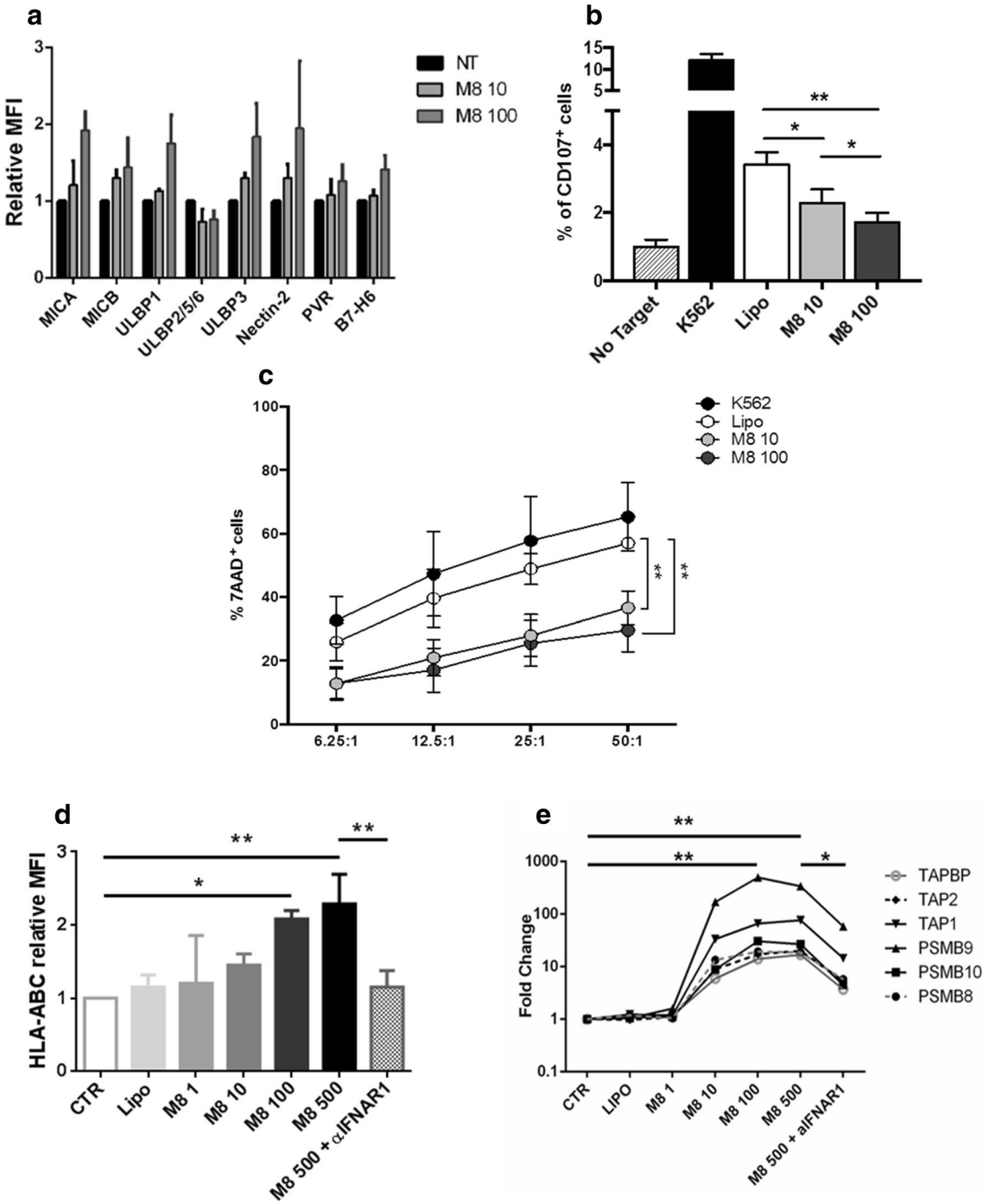

Fig. 5 M8 triggering of RIG-I represses NK-mediated cancer cell killing and activates antigen processing machinery. **a** Relative expression levels of NK activating ligands on Mel1007 transfected with M8 (10–100 ng/ml) for 48 h; **b** degranulation assay of NK from healthy donors co-cultured with Mel1007 cells transfected with M8 (10–100 ng/ml) for 48 h. Data are represented as mean values of the percentage of CD107a + cells ± SEM; **c** cytotoxicity assay of NKL cell line against Mel1007 cells transfected with M8 (10–100 ng/ml) for 48 h. Mean ± SEM values are shown. Both in **b** and **c** K562 were used as a positive control of NK activation; **d** MFI of HLA-ABC expression levels of Mel1007 transfected for 24 h with different doses of M8 (1–500 ng/ml) and IFNAR1 blocking Ab (1 µg/ml) over control cells; **e** expression levels of the indicated APM genes in Mel1007 cells 24 h after transfection with different doses of M8 (1–500 ng/ml) and IFNAR1 blocking Ab (1 µg/ml) over control cells. $*P < 0.05$; $**P < 0.01$

The expression of numerous APM genes—immunoproteasome subunits PSMB8, PSMB9, and PSMB10, transporters associated with antigen processing TAP1 and TAP2, and the endoplasmic reticulum chaperone Tapasin (TAPBP)—displayed a dose-dependent increase in M8-Mel1007 cells, peaking at a concentration of 100 ng/ml M8, with induction ranging from 15- to 500-fold, relative to untreated cells (Fig. 5e). Consistent with previous studies [20], the expression of APM factors was strongly dependent on IFN-I, since IFNAR1 signaling blockade resulted in a reduction of the expression levels of both HLA-ABC protein (to basal levels) and APM genes (~three–sixfold) (Fig. 5d, e). Similar results in terms of reduced NK activity and APM induction were also observed in HCT116 cells (data not shown). Altogether, these results indicate that the antigen processing machinery was activated in an IFN-dependent manner in cancer cells treated with M8, whereas anti-tumor NK activity was inhibited.

Dendritic cell activation is skewed toward a pro-inflammatory phenotype

Based on the induction of ICD-DAMP and APM activation in M8-Mel1007, we next examined DC activity to determine whether the immune stimulatory signals induced by M8 also enhanced DC phagocytosis of M8-Mel1007. Monocyte-derived DC (MoDC) co-cultured with labeled Mel1007 or M8-Mel1007 were evaluated for their ability to incorporate membrane dye by phagocytosis. Strikingly, MoDC phagocytized significantly more M8 treated-Mel1007 cells compared to control Mel1007 (9.5% vs 2.2%) (Fig. 6a, b).

Next, we evaluated whether immune stimulatory signals induced in M8-Mel1007 cells affected the DC phenotype, specifically expression of co-stimulatory markers and cytokine production. Flow cytometric analyses showed that supernatants of M8-Mel1007 administered to DC increased the expression levels of co-stimulatory markers CD80 and CD86, and of HLA-DR of ~2.2-, 4.7-, and 2-fold, respectively, thus indicating an increased potential to stimulate T cell activation (Fig. 6c). Moreover, expression of the pro-Th1 cytokine IL-12 was stimulated in DC, whereas levels of the pro-Treg cytokine IL-10 remained unchanged (Fig. 6d). The pro-inflammatory cytokine CXCL10 was stimulated by M8-Mel1007 in a dose-dependent manner (Fig. 6e), further supporting the observation that M8 treatment of Mel1007 stimulated the phagocytic potential of DC and also directed DC towards a pro-inflammatory phenotype.

Discussion

Immunotherapy has emerged as a fourth pillar of cancer treatment—together with chemotherapy, radiation and surgery—to revolutionize clinical cancer care. Several immunotherapeutic strategies have reached clinical practice and demonstrated durable clinical responses and improved survival [38–40]. However, the efficacy of these strategies is limited to patients with highly immunogenic tumors; while for the majority of patients, complementary therapeutic strategies are required to convert non-immunogenic ("cold") tumors into immunogenic ("hot") tumors.

Immune mechanisms targeted against viral infection rely on recognition of viral components (often viral nucleic acids with distinct PAMP) to initiate a complex, multifaceted array of processes that includes the secretion of IFN-I and chemokines to mobilize immune effector cells, the activation of the APM for immune recognition of non-self antigens, and in the last instance, cell death. All these processes are also critical for the development of an efficient cancer immunotherapy. In the present study, we demonstrate that a sequence-optimized RIG agonist—M8 [16, 17] induced ICD-DAMP in cancer cell lines and triggered intrinsic apoptotic pathways by an IFN-I-dependent mechanism. Moreover, M8 boosted HLA-ABC and APM expression, and activated DC toward a more pro-inflammatory phagocytic phenotype. M8 outperformed other RA in the induction of antiviral signaling [16], and potentiation of immune response [17], with an efficacy dependent on an intact RIG-I pathway and on the preservation of the 5′ triphosphate moiety. Taken together, our results highlight M8 as a promising, broad-acting RA for cancer immunotherapy against multiple tumor types. Nevertheless, additional studies are necessary to identify experimental conditions in which RIG-I activation is desirable.

IFN-I plays a critical role in the development of the anti-tumor response because of its capacity to induce ICD on tumor cells [19], in part due to the induction of the pro-apoptotic BH-3 only proteins NOXA and PUMA [21–27]. Tumor cells often develop resistance to IFN-I signaling by downregulating IFNAR1 surface receptor expression or by altering downstream signaling intermediates [22, 23, 28, 29], although some IFN-I signals are minimally affected by IFNAR1 levels [30]. In the present experiments, cell death induced by M8 relied on IFN-I production, and blockade of IFNAR1 signaling decreased cancer cell death. Other RA have demonstrated the ability to induce both IFN-dependent and -independent mechanisms of cell death [11, 12], that may be due to cell-specific differences in the induction of antiviral versus apoptotic responses. Whether the effects of M8 would be limited in tumor cells with defective IFN-I responses should be explored in more depth. Strategies such as oncolytic virotherapy that specifically take advantage of defects in IFN-I signaling would potentially be more effective in settings of diminished IFN responses [31–33].

NK cells exert a crucial role in modulating the response to cancer therapy in several settings [34, 35]. However, contrasting results have been reported on the relevance of

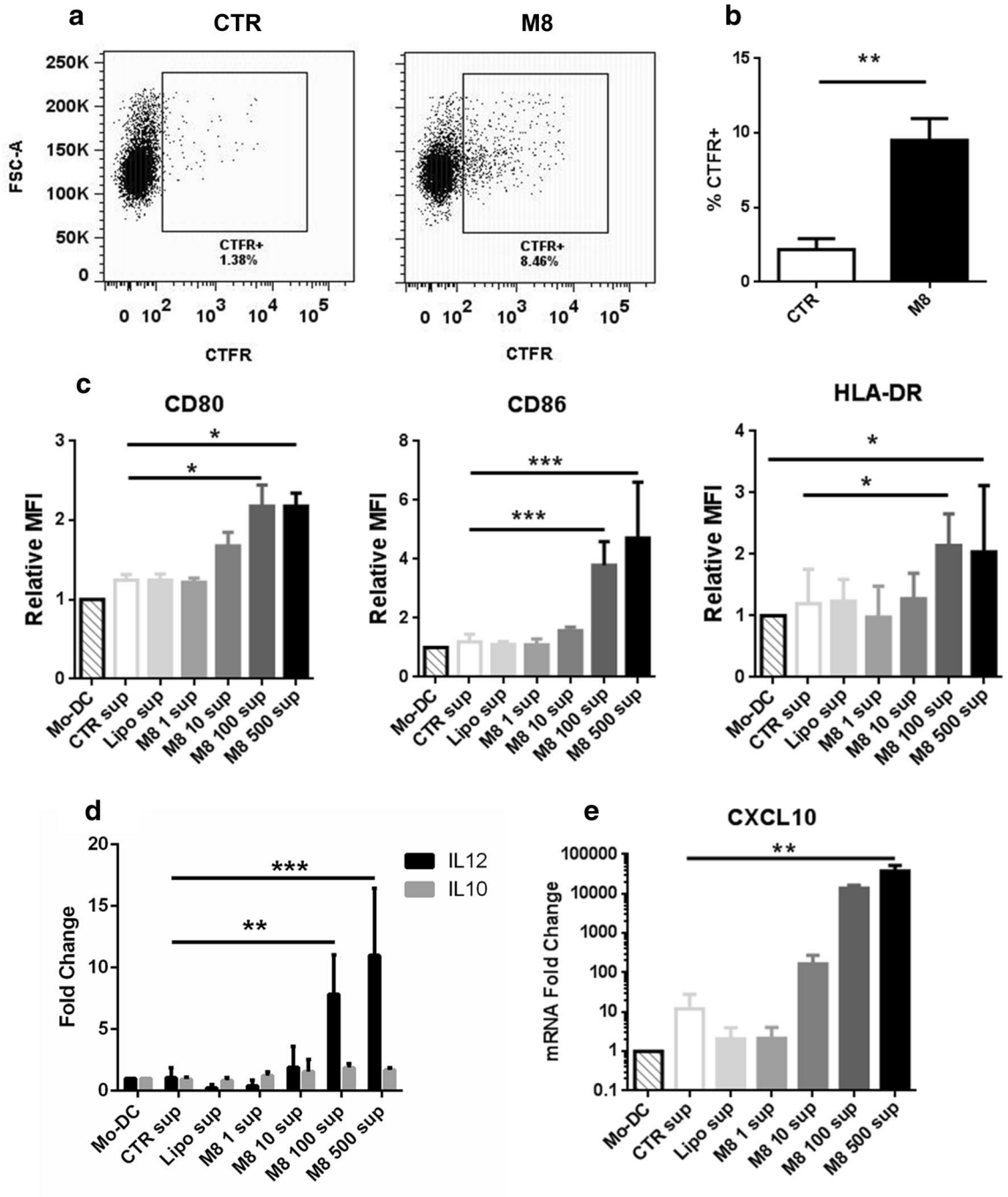

Fig. 6 M8 treatment in cancer cells induces phagocytosis and pro-inflammatory phenotype in DC. **a**, **b** Mel1007 cells were stained with CTFR and then transfected with M8 (500 ng/ml). After 48 h, Mo-DC were added to the cell culture at a 1:1 ratio. After 4 h, phagocytosis of DC was assessed by flow cytometry, analyzing the percentage of DC (gated on CD209 expression) that incorporated CTFR. **a** Representative plots of the phagocytosis assay; **b** percentage of DC phagocytosis as in **a**; **c**–**e** effects of supernatants of transfected Mel1007 cells on DC. Mel1007 were transfected for 48 h with different doses of M8 (1–500 ng/ml), supernatants were then used to stimulate DC. **c** Cell surface expression levels expressed as relative MFI of co-stimulatory markers CD80 and CD86 and HLA-DR in DC treated for 24 h with supernatants of Mel1007 transfected with different doses of M8; **d**, **e** expression levels of IL-12A, IL-10 and CXCL10 genes in DC treated as in c). $^{*}P<0.05$; $^{**}P<0.01$; $^{***}P<0.001$

NK cells in RA-based immunotherapy [11, 13, 14, 36]. In contrast to other groups that analyzed systemic NK activation [11] or the activating effect of cell supernatants [13], our results showed an overall inhibition of NK cell activity against M8-transfected cells, despite the increased expression of several NK activating ligands. We believe

this may be due to the strong overexpression of the inhibitory ligand HLA-ABC, but additional factors could also be involved. Whether reduced NK activity would affect M8-based immunotherapy will be evaluated in vivo in the near future to obtain a detailed understanding of mechanisms regulating NK activity upon RA treatment.

The generation and/or strengthening of anti-tumor antigen-specific immune responses is considered the foundations of successful cancer immunotherapy, particularly given the progress with immune checkpoint inhibitor therapies [37–39]. Because of their ability to actively uptake and process tumor antigens, DC play a pivotal role in inducing and maintaining tumor-specific T cell responses [40] and combination therapies aimed at increasing the pool of tumor antigens recognized by T cells are highly sought after strategies [41]. Our observations that M8-treated tumor cells are phagocytized by DC, and that DC stimulated with supernatants from M8-treated cells increased the expression of HLA-DR and costimulatory molecules, and promoted pro-inflammatory cytokine production, indicate that M8 immunotherapy could broaden the anti-tumor antigenic repertoire. Also, the upregulation of the APM in cancer cells by M8 could increase the recognition of cancer cells by the tumor infiltrating lymphocytes, and thus additionally favor a strong antigen-specific T cell-mediated immune response.

During the final preparation of this study, we became aware of an excellent study that evaluated a distinct engineered RA in a breast cancer cell panel that represented each of three major clinical breast cancer subtypes [42]. Notably, in this setting, the RA triggered the extrinsic apoptosis pathway and pyroptosis, and also induced expression of lymphocyte-recruiting chemokines and IFN-I. Importantly, RIG-I activation in breast tumors increased tumor lymphocytes and decreased tumor growth and metastasis, thus illustrating the successful therapeutic delivery of a synthetic RA to induce breast tumor cell killing and to modulate the tumor microenvironment in vivo.

In conclusion, we report that an optimized RA M8 induced IFN-I dependent apoptosis in several tumor cell lines, characterized by the production of ICD-DAMP, together with the activation of APM and DC. These results demonstrate that M8 triggering of the RIG-I pathway activates multiple processes within the tumor microenvironment that favors the induction and strength of antigen-specific responses and could synergize with checkpoint inhibitors. Whether these effects will be sufficient for effective tumor treatment will be explored in future in vivo studies.

Author contributions Conception and design: LC, AZ, JH, DO. Collection and assembly of data: LC, AZ, EV, MM, MF, EP, GP, CK. Data analysis and interpretation: LC, MJ, DO, AZ, AS, and JH. Manuscript writing: LC, AZ, JH. Final approval of manuscript: all authors.

Funding This research was supported by grants from Fondazione Cenci Bolognetti, the Italian Association for Cancer Research (AIRC) (IG16901), and NIH Grants 1R561AI108861-01A1 and 7R21CA192185. Elisabetta Vulpis is supported by an AIRC fellowship for Italy.

Compliance with ethical standards

Conflict of interest The authors declare that they have no conflict of interest.

Informed consent PBMC were freshly isolated from peripheral blood samples of anonymous volunteer healthy donors at the Transfusion Center of Sapienza University of Rome. Written informed consent was obtained from all blood donors to the use of their blood for scientific purposes.

Ethical approval All procedures performed in studies involving human participants were in accordance with the ethical standards of the Ethics Committee of the Sapienza University of Rome (Rif.3373/250914) and with the 1964 Helsinki declaration. Institutional Review Board approval was not required for this kind of study.

Cell line authentication Primary Mel1007 and metastatic melanoma Mel120 cells were a kind gift of Dr. G. Parmiani (Milan, Italy), A549, HCT116 and PC3 were all from ATCC. All the experiments were performed with cells at low passage numbers (≤ 10). Cell identity was monitored based on morphology and growth rate. Mycoplasma was routinely tested.

References

1. Schreiber RD, Old LJ, Smyth MJ (2011) Cancer immunoediting: integrating immunity's roles in cancer suppression and promotion. Science 331:1565–1570
2. Mittal D, Gubin MM, Schreiber RD, Smyth MJ (2014) New insights into cancer immunoediting and its three component phases—elimination, equilibrium and escape. Curr Opin Immunol 27:16–25. https://doi.org/10.1016/j.coi.2014.01.004
3. Iurescia S, Fioretti D, Rinaldi M (2018) Targeting cytosolic nucleic acid-sensing pathways for cancer immunotherapies. Front Immunol 9:711. https://doi.org/10.3389/fimmu.2018.00711
4. Hornung V, Ellegast J, Kim S et al (2006) 5′-Triphosphate RNA is the ligand for RIG-I. Science 314:994–997. https://doi.org/10.1126/science.1132505
5. Kawai T, Takahashi K, Sato S et al (2005) IPS-1, an adaptor triggering RIG-I- and Mda5-mediated type I interferon induction. Nat Immunol 6:981–988. https://doi.org/10.1038/ni1243
6. Goulet M-LL, Olagnier D, Xu Z et al (2013) Systems analysis of a RIG-I agonist inducing broad spectrum inhibition of virus infectivity. PLoS Pathog 9:e1003298. https://doi.org/10.1371/journal.ppat.1003298
7. Zevini A, Olagnier D, Hiscott J (2017) Crosstalk between cytoplasmic RIG-I and STING sensing pathways. Trends Immunol 38:194–205
8. Heylbroeck C, Balachandran S, Servant MJ et al (2000) The IRF-3 transcription factor mediates Sendai virus-induced

apoptosis. J Virol 74:3781–3792. https://doi.org/10.1128/JVI.74.8.3781-3792.2000
9. Chattopadhyay S, Kuzmanovic T, Zhang Y et al (2016) Ubiquitination of the transcription factor IRF-3 activates RIPA, the apoptotic pathway that protects mice from viral pathogenesis. Immunity 44:1151–1161. https://doi.org/10.1016/j.immuni.2016.04.009
10. Schock SN, Chandra NV, Sun Y et al (2017) Induction of necroptotic cell death by viral activation of the RIG-I or STING pathway. Cell Death Differ 24:615–625. https://doi.org/10.1038/cdd.2016.153
11. Poeck H, Besch R, Maihoefer C et al (2008) 5′-Triphosphate-siRNA: turning gene silencing and Rig-I activation against melanoma. Nat Med 14:1256–1263. https://doi.org/10.1038/nm.1887
12. Besch R, Poeck H, Hohenauer T et al (2009) Proapoptotic signaling induced by RIG-I and MDA-5 results in type I interferon–independent apoptosis in human melanoma cells. J Clin Investig 119:2399–2411. https://doi.org/10.1172/JCI37155
13. Glas M, Coch C, Trageser D et al (2013) Targeting the cytosolic innate immune receptors RIG-I and MDA5 effectively counteracts cancer cell heterogeneity in glioblastoma. Stem Cells 31:1064–1074. https://doi.org/10.1002/stem.1350
14. Ellermeier J, Wei J, Duewell P et al (2013) Therapeutic efficacy of bifunctional siRNA combining TGF-1 silencing with RIG-I activation in pancreatic cancer. Cancer Res 73:1709–1720. https://doi.org/10.1158/0008-5472.CAN-11-3850
15. Duewell P, Steger A, Lohr H et al (2014) RIG-I-like helicases induce immunogenic cell death of pancreatic cancer cells and sensitize tumors toward killing by CD8+ T cells. Cell Death Differ 21:1825–1837. https://doi.org/10.1038/cdd.2014.96
16. Chiang C, Beljanski V, Yin K et al (2015) Sequence-specific modifications enhance the broad-spectrum antiviral response activated by RIG-I agonists. J Virol 89:8011–8025. https://doi.org/10.1128/JVI.00845-15
17. Beljanski V, Chiang C, Kirchenbaum GA et al (2015) Enhanced influenza virus-like particle vaccination with a structurally optimized RIG-I agonist as adjuvant. J Virol 89:10612–10624. https://doi.org/10.1128/JVI.01526-15
18. Zingoni A, Palmieri G, Morrone S et al (2000) CD69-triggered ERK activation and functions are negatively regulated by CD94/NKG2-A inhibitory receptor. Eur J Immunol 30:644–651. https://doi.org/10.1002/1521-4141(200002)30:2%3c644:AID-IMMU644%3e3.0.CO;2-H
19. Galluzzi L, Buqué A, Kepp O et al (2017) Immunogenic cell death in cancer and infectious disease. Nat Rev Immunol 17:97–111. https://doi.org/10.1038/nri.2016.107
20. Leone P, Shin E-C, Perosa F et al (2013) MHC class I antigen processing and presenting machinery: organization, function, and defects in tumor cells. JNCI J Natl Cancer Inst 105:1172–1187. https://doi.org/10.1093/jnci/djt184
21. Dunn GP, Bruce AT, Sheehan KCF et al (2005) A critical function for type I interferons in cancer immunoediting. Nat Immunol 6:722–729. https://doi.org/10.1038/ni1213
22. Katlinskaya YV, Katlinski KV, Yu Q et al (2016) Suppression of type I interferon signaling overcomes oncogene-induced senescence and mediates melanoma development and progression. Cell Rep 15:171–180. https://doi.org/10.1016/J.CELREP.2016.03.006
23. Katlinski KV, Gui J, Katlinskaya YV et al (2017) Inactivation of interferon receptor promotes the establishment of immune privileged tumor microenvironment. Cancer Cell 31:194–207. https://doi.org/10.1016/j.ccell.2017.01.004
24. Castiello L, Sestili P, Schiavoni G et al (2018) Disruption of IFN-I signaling promotes HER2/Neu tumor progression and breast cancer stem cells. Cancer Immunol Res 6:658–670. https://doi.org/10.1158/2326-6066.CIR-17-0675
25. Rizza P, Moretti F, Capone I, Belardelli F (2015) Role of type I interferon in inducing a protective immune response: perspectives for clinical applications. Cytokine Growth Factor Rev 26:195–201. https://doi.org/10.1016/j.cytogfr.2014.10.002
26. Gajewski TF, Fuertes MB, Woo S-R (2012) Innate immune sensing of cancer: clues from an identified role for type I IFNs. Cancer Immunol Immunother 61:1343–1347. https://doi.org/10.1007/s00262-012-1305-6
27. Snell LM, Mcgaha TL, Brooks DG (2017) Type I interferon in chronic virus infection and cancer. Trends Immunol 38:542–557. https://doi.org/10.1016/j.it.2017.05.005
28. HuangFu W-C, Qian J, Liu C et al (2012) Inflammatory signaling compromises cell responses to interferon alpha. Oncogene 31:161–172. https://doi.org/10.1038/onc.2011.221
29. Bhattacharya S, HuangFu W-C, Dong G et al (2013) Anti-tumorigenic effects of Type 1 interferon are subdued by integrated stress responses. Oncogene 32:4214–4221. https://doi.org/10.1038/onc.2012.439
30. Levin D, Harari D, Schreiber G (2011) Stochastic receptor expression determines cell fate upon interferon treatment. Mol Cell Biol 31:3252–3266. https://doi.org/10.1128/MCB.05251-11
31. Stojdl DF, Lichty BD, tenOever BR et al (2003) VSV strains with defects in their ability to shutdown innate immunity are potent systemic anti-cancer agents. Cancer Cell 4:263–275
32. Nguyen TL-A, Abdelbary H, Arguello M et al (2008) Chemical targeting of the innate antiviral response by histone deacetylase inhibitors renders refractory cancers sensitive to viral oncolysis. Proc Natl Acad Sci 105:14981–14986. https://doi.org/10.1073/pnas.0803988105
33. Olagnier D, Lababidi RR, Hadj SB et al (2017) Activation of Nrf2 signaling augments vesicular stomatitis virus oncolysis via autophagy-driven suppression of antiviral immunity. Mol Ther 25:1900–1916. https://doi.org/10.1016/j.ymthe.2017.04.022
34. Sanchez-Correa B, Morgado S, Gayoso I et al (2011) Human NK cells in acute myeloid leukaemia patients: analysis of NK cell-activating receptors and their ligands. Cancer Immunol Immunother 60:1195–1205. https://doi.org/10.1007/s00262-011-1050-2
35. Zingoni A, Fionda C, Borrelli C et al (2017) Natural killer cell response to chemotherapy-stressed cancer cells: role in tumor immunosurveillance. Front Immunol 8:1194. https://doi.org/10.3389/fimmu.2017.01194
36. Barsoum J, Renn M, Schuberth C, et al (2017) Abstract B44: Selective stimulation of RIG-I with a novel synthetic RNA induces strong anti-tumor immunity in mouse tumor models. In: Cancer Immunology Research. American Association for Cancer Research, pp B44–B44
37. Ribas A, Wolchok JD (2018) Cancer immunotherapy using checkpoint blockade. Science 359:1350–1355
38. Rizvi NA, Hellmann MD, Snyder A et al (2015) Mutational landscape determines sensitivity to PD-1 blockade in non-small cell lung cancer. Science 348:124–128. https://doi.org/10.1126/science.aaa1348
39. Van Allen EM, Miao D, Schilling B et al (2015) Genomic correlates of response to CTLA-4 blockade in metastatic melanoma. Science 350:207–211. https://doi.org/10.1126/science.aad0095
40. Zong J, Keskinov AA, Shurin GV, Shurin MR (2016) Tumor-derived factors modulating dendritic cell function. Cancer Immunol Immunother 65:821–833. https://doi.org/10.1007/s00262-016-1820-y
41. Schumacher TN, Schreiber RD (2015) Neoantigens in cancer immunotherapy. Science 348:69–74. https://doi.org/10.1126/science.aaa4971
42. Elion DL, Jacobson ME, Hicks DJ et al (2018) Therapeutically active RIG-I agonist induces immunogenic tumor cell killing in breast cancers. Cancer Res. https://doi.org/10.1158/0008-5472.CAN-18-0730